Nondipole effects in the angular distribution of photoelectrons in two-photon two-color above-threshold atomic ionization

A. N. Grum-Grzhimailo and E. V. Gryzlova
Skobeltsyn Institute of Nuclear Physics, Lomonosov Moscow State University, Moscow 119991, Russian Federation
(Received 20 February 2014; published 23 April 2014)

Expressions for the angular distribution of photoelectrons produced in two-photon two-color atomic ionization are obtained within the statistical tensor formalism, taking into account a full multipole expansion of the radiation in electric and magnetic moments. The general expressions are reduced to a simpler form for a particular geometry used in experiments with XUV + optical radiation beams and analyzed within the first-order nondipole corrections for different polarization states of the photons. As a numerical example, the Ne 1*s* above-threshold ionization by two-color radiation is considered within the second-order perturbation theory. A large forward-backward asymmetry in the photoelectron angular distribution is predicted.

DOI: 10.1103/PhysRevA.89.043424 PACS number(s): 32.80.Rm, 32.80.Wr, 32.80.Fb

I. INTRODUCTION

Multiphoton atomic ionization has been studied extensively for decades. These studies are important for the fundamental understanding of nonlinear processes and also for applications. The modern theory describing nonlinear photoprocesses was developed for atoms in strong optical or UV laser fields and is based on the electric dipole ($E1$) approximation for the atom-field interaction. It is believed that the dipole approximation is appropriate for fields of moderate intensity when the radiation wavelength is much larger than the size of the atom, provided the dipole transitions are not forbidden by selection rules. Ionization probabilities and angular distributions of electrons emitted in multiphoton ionization processes are discussed within the dipole approximation in many review papers and monographs, for example [1–5]. Until recently, however, the study of nondipole (retardation) effects in atomic multiphoton ionization was restricted to the special case of resonant ionization by a monochromatic field in the optical region, with emphasis to ionization close to resonance with a discrete atomic level ([6–9] and references therein). With the advent of free-electron lasers (FELs) generating intense short-wavelength femtosecond pulses, nonlinear processes in the XUV and x-ray wavelength range became accessible experimentally [10], thus stimulating further investigations of the nondipole effects in the nonlinear processes.

Since the early years of quantum mechanics ([11] and references therein), it is known that for atomic hydrogen the retardation corrections to the single-photon absorption cross section, which is due to the $\boldsymbol{A}\cdot\boldsymbol{p}$ term of the Hamiltonian (where $\boldsymbol{A}$ is the vector potential in the Coulomb gauge and $\boldsymbol{p}$ is the electron momentum operator), become noticeable only at near-relativistic energies. On the other hand, due to interference between partial-wave amplitudes, which does not occur in the total cross section, these corrections modify the photoelectron angular distribution (PAD) at much lower energies than they affect the angle-integrated cross sections. Turning to heavier atoms, it is known that in ionization of some subshells already at photon energies of a few hundred eV, in special cases even less, the angular distribution and spin polarization of the photoelectrons in single-photon atomic ionization are affected significantly by interference between the electric dipole and electric quadrupole ($E2$) amplitudes [contributions from magnetic dipole ($M1$) transitions to the continuum are normally negligible] [12–14]. In ionization of inner atomic shells, when the photon energy is of the order of keV and even higher, the nondipole corrections to the PAD sometimes show up already just above the ionization threshold [15–19]. For such cases, nondipole effects should be present in the XUV or x-ray nonlinear atomic processes at similar energies, since at least for one of the absorbed photons similar atomic continua and similar transitions are involved as in single-photon ionization.

Recently, retardation effects were considered theoretically in the two-photon monochromatic above-threshold ionization (ATI) of hydrogenlike atoms in the x-ray regime [20–23]. Calculations of [23] confirmed the dominance of the first-order nondipole corrections to the PADs originating from the terms proportional to $\boldsymbol{k}\cdot\boldsymbol{p}$, where $\boldsymbol{k}$ is the photon momentum, at least for photon energies up to 1 keV, and the dominance of the $\boldsymbol{A}\cdot\boldsymbol{p}$ contribution in comparison with the $\boldsymbol{A}^2$ contribution. Taking advantage of the exactly known nonrelativistic wave functions of the hydrogen atom and hydrogenlike ions, it was possible, within second-order perturbation theory, to obtain analytical results for the amplitudes of the two-photon monochromatic ionization, including all multipoles of the electromagnetic field [23]. PADs in the two-photon monochromatic ionization of hydrogenlike ions below the ATI threshold, but including all field multipoles, were treated within the relativistic second-order perturbation theory and using the density-matrix approach in [24]. For highly charged hydrogenlike ions (Xe^{53+}, U^{91+}), strong retardation effects in the PADs were found for circular, linear, and unpolarized photon beams.

In systems with two or more electrons, absorption of two x-ray photons proceeds sequentially with the formation of an intermediate ionic state with much higher probability than the two-photon ATI [25,26] process, provided the photon energy is larger than the ionization energy of the singly charged ion. In recent papers [27,28], nondipole effects in the PAD in sequential two-photon double ionization were considered. Another situation, in which the nondipole corrections could be important, is the two-color (XUV + optical) ionization, when the XUV photon generates the nondipole transitions to the atomic continuum, which are then monitored and possibly

controlled by the optical photon. Two-color two-photon ATI is the subject of experiments with high harmonics [29–38] and free-electron lasers [39–42], supported by theoretical studies within the dipole approximation (for example [42–46]). A very important aspect of the two-photon two-color ionization is the polarization dependence of the cross sections, since the polarization of the optical laser is easily variable and is used as an advantage when extracting information on the dynamics of the process [40,41]. It is the purpose of this paper to work out an approach to the PAD in multiphoton multicolor atomic ionization beyond the dipole approximation and to specifically apply it to two-photon two-color ionization within the lowest-order nondipole corrections. In order to obtain general expressions for the PADs, we extend previous work on one-photon atomic ionization in the dipole [47] and nondipole [48] approximations based on the statistical tensor formalism.

The structure of this manuscript is as follows. A general expression for the PAD in multiphoton multicolor ionization without restricting the field multipoles is presented in Sec. II in terms of geometrical and dynamical factors. Section III specifies the geometrical and dynamical factors for the two-photon ionization process. As a particular application, angular distributions in the two-photon two-color ionization within the first-order nondipole corrections are derived in Sec. IV for parallel photon beams. A numerical example is given in Sec. V for the XUV + optical laser 1s ionization of atomic Ne within the second-order perturbation theory.

Unless stated otherwise, we use atomic units throughout this paper.

II. GENERAL CONSIDERATIONS

Consider the multiphoton multicolor atomic ionization

$$[\gamma(\omega_1,P_1,\Omega_1)+\gamma(\omega_2,P_2,\Omega_2)+\cdots+\gamma(\omega_n,P_n,\Omega_n)] + A(\alpha_0 J_0) \longrightarrow [A^+(\alpha_f J_f)] + e^-(\boldsymbol{p}) \tag{1}$$

by n photons with arbitrary polarizations, characterized by triads of their Stokes parameters $P_i \equiv \{p_1^{(i)},p_2^{(i)},p_3^{(i)}\}$, directions of propagation $\Omega_i \equiv \{\theta_i,\phi_i\}$ in the laboratory frame, and frequencies ω_i $(i=1,2,\ldots,n)$. We denote by $[A^+(\alpha_f J_f)]$ the final complex consisting of the nuclei and $N-1$ electrons (some of which may be in the continuum), where N is the number of electrons in the initial atomic state $A(\alpha_0 J_0)$. The initial state of the atom and the final state of the complex are characterized by the total angular momenta J_0 and J_f, respectively, with sets of other quantum numbers α_0 and α_f specifying the states. The photoelectron linear momentum $\boldsymbol{p}$ is determined by the photoelectron energy ε, $p=\sqrt{2\varepsilon}$, and the direction of the electron propagation $\{\vartheta,\varphi\}$.

We assume that the photon pulses contain many optical cycles and that the photon beams are mutually incoherent. Therefore, the effects of the pulse shapes, relative phases of the electromagnetic fields, time delay, and coherence between the pulses are irrelevant in our treatment of the PADs, and thus the nondipole contribution to such phenomena as streaking, carrier envelope phase effects, and other processes for which the time dependence of the electromagnetic field is crucial, is beyond the scope of the present manuscript. The radiation field is treated classically and its corresponding multipole expansion will be used.

Formulas for the PADs can be obtained by employing the statistical tensor formalism [49–51] within a stationary approach, in close similarity to earlier work [47,48], where single-photon ionization was treated. New features compared to [47,48] when deriving a general expression for the PAD are the construction of statistical tensors of n incoming photons from statistical tensors of the individual photons and introducing amplitudes for multiphoton transitions.

Following almost literally Eqs. (6)–(14) of [47], except for replacing the statistical tensors of a single photon by those of n incoming photons and substituting the one-photon dipole transition matrix element by a general transition matrix element describing the n-photon transition without restricting the field multipoles, we obtain for the PAD in the n-photon absorption

$$W(\vartheta,\varphi)=\sum_{k_0 k k_\gamma}\sum_{\substack{\alpha_\gamma\alpha'_\gamma\\ L_\gamma L'_\gamma}} B^{n\gamma}_{k_0 k k_\gamma}(\alpha_\gamma L_\gamma,\alpha'_\gamma L'_\gamma) \times F^{n\gamma}_{k_0 k k_\gamma}(\alpha_\gamma L_\gamma,\alpha'_\gamma L'_\gamma;\vartheta,\varphi;\{P,\Omega\}). \tag{2}$$

Here the multiphoton dynamical and geometrical factors are, respectively, of the form

$$\begin{aligned} &B^{n\gamma}_{k_0 k k_\gamma}(\alpha_\gamma L_\gamma,\alpha'_\gamma L'_\gamma) \\ &= 3\hat{J}_0\sum_{\substack{\ell\ell' jj'\\ JJ'}}(-1)^{J+J_f+k_\gamma-1/2}\hat{J}\hat{J}'\hat{j}\hat{j}'\hat{\ell}\hat{\ell}'(\ell 0,\ell' 0\,|\,k0) \\ &\times\begin{Bmatrix} J & J' & k\\ j' & j & J_f\end{Bmatrix}\begin{Bmatrix} j & j' & k\\ \ell' & \ell & \frac{1}{2}\end{Bmatrix}\begin{Bmatrix} J_0 & L_\gamma & J\\ J_0 & L'_\gamma & J'\\ k_0 & k_\gamma & k\end{Bmatrix} \\ &\times\langle\alpha_f J_f,\ell j: J\,||\,T\,||\,\alpha_0 J_0,\alpha_\gamma L_\gamma: J\rangle \\ &\times\langle\alpha_f J_f,\ell' j': J'\,||\,T\,||\,\alpha_0 J_0,\alpha'_\gamma L'_\gamma: J'\rangle^* \end{aligned} \tag{3}$$

and

$$\begin{aligned} &F^{n\gamma}_{k_0 k k_\gamma}(\alpha_\gamma L_\gamma,\alpha'_\gamma L'_\gamma;\vartheta,\varphi;\{P,\Omega\}) \\ &= \sqrt{4\pi}\hat{k}_0\sum_{q_\gamma}\left\{\rho^*_{k_0}(\alpha_0 J_0)\otimes Y_k(\vartheta,\varphi)\right\}_{k_\gamma q_\gamma} \\ &\times\rho^{n\gamma}_{k_\gamma q_\gamma}(\alpha_\gamma L_\gamma,\alpha'_\gamma L'_\gamma;\{P;\Omega\}). \end{aligned} \tag{4}$$

The summation in Eq. (2) is over the total angular momentum of the n photons L_γ and other quantum numbers α_γ specifying the state of the n photons; α_γ includes the set of the field multipoles and intermediate couplings of the photon's angular momenta. The set of photon polarizations and the directions of the photon beams are denoted as $\{P;\Omega\}$: $\{P;\Omega\}\equiv\{P_1,P_2,\ldots,P_n;\Omega_1,\Omega_2,\ldots,\Omega_n\}$. Below we will omit the polarization and direction of propagation of the photons in the arguments of the statistical tensors and the geometrical factors for brevity, unless such omission would lead to confusion. In Eqs. (3) and (4), ℓ and j stand for the orbital and total angular momenta of the photoelectron, respectively, we have abbreviated $\hat{a}=\sqrt{2a+1}$, and standard notations are used for the spherical harmonics, the tensorial product, Clebsch-Gordon coefficients, and nj coefficients [52]. The Condon-Shortley phase convention is implied, the angular

momenta are coupled from left to right, and $\boldsymbol{j} = \boldsymbol{\ell} + \boldsymbol{s}$. The transition matrix elements for multiphoton ionization in Eq. (3) need special treatment. However, it is only important here that they enter the PAD as angle-independent quantities. The statistical tensors $\rho_{k_0 q_0}(\alpha_0 J_0)$ describe the polarization of the initial atomic state. The n-photon statistical tensors $\rho^{n\gamma}_{k_\gamma q_\gamma}(\alpha_\gamma L_\gamma, \alpha'_\gamma L'_\gamma)$ can be built from those of the individual photons, as will be exemplified in the next section. They obey the general relation

$$\rho^{n\gamma}_{k_\gamma q_\gamma}(\alpha_\gamma L_\gamma, \alpha'_\gamma L'_\gamma) = (-1)^{L'_\gamma - L_\gamma + q_\gamma} \left[\rho^{n\gamma}_{k_\gamma - q_\gamma}(\alpha'_\gamma L'_\gamma, \alpha_\gamma L_\gamma)\right]^*, \tag{5}$$

expressing the fact that the density matrix of n photons is Hermitian. It is implied in Eq. (4) that the n-photon statistical tensor and the statistical tensors of the atom are given in the same coordinate system. At the same time the n-photon geometrical factors (4) are rotationally invariant as a scalar product of two tensors. For an unpolarized initial atomic state [$\rho_{k_0 q_0}(\alpha_0 J_0) = \delta_{k_0 0}\delta_{q_0 0}\hat{J}_0^{-1}$] Eq. (4) reduces to

$$F^{n\gamma}_{k_0 k k_\gamma}(\alpha_\gamma L_\gamma, \alpha'_\gamma L'_\gamma) = \delta_{0 k_0}\delta_{k k_\gamma}\sqrt{4\pi}\,\hat{J}_0^{-1} \sum_q Y_{kq}(\vartheta,\varphi)\rho^{n\gamma}_{kq}(\alpha_\gamma L_\gamma, \alpha'_\gamma L'_\gamma). \tag{6}$$

Equations (3) and (4) are a generalization of Eqs. (13) and (14) of [47], respectively, to an arbitrarily polarized initial atomic state, an arbitrary number of photon beams, and arbitrary field multipoles.

The geometrical factors (4) depend on the number of photon beams, their polarizations, the directions of propagation and photon multipolarities, the polarization of the initial atomic state, and the direction of the photoemission. They do not depend on the details of the atomic structure and dynamics of the photon-atom interaction, which are included in the dynamical factors (3). Permutation of primed and not primed summation indices yields the relations

$$B^{n\gamma}_{k_0 k k_\gamma}(\alpha_\gamma L_\gamma, \alpha'_\gamma L'_\gamma) = (-1)^{L_\gamma + L'_\gamma + k_0 + k_\gamma + k}\left[B^{n\gamma}_{k_0 k k_\gamma}(\alpha'_\gamma L'_\gamma, \alpha_\gamma L_\gamma)\right]^*, \tag{7}$$

$$F^{n\gamma}_{k_0 k k_\gamma}(\alpha_\gamma L_\gamma, \alpha'_\gamma L'_\gamma) = (-1)^{L_\gamma + L'_\gamma + k_0 + k_\gamma + k}\left[F^{n\gamma}_{k_0 k k_\gamma}(\alpha'_\gamma L'_\gamma, \alpha_\gamma L_\gamma)\right]^*. \tag{8}$$

Relations (7) and (8) ensure real values for the PAD (2). Additional relationships between the coefficients (3) follow from parity conservation. (An example for the two-photon ionization will be given in Sec. III.) In principle, general symmetry properties of the factors (3) and (4) allow us to find appropriate parametrizations for the PADs. Some examples will be provided in Sec. IV.

The PAD (2) is related to a differential "generalized cross section"

$$\frac{d\sigma}{d\Omega} = cW(\vartheta,\varphi), \tag{9}$$

where the factor c normalizes the probability to unit photon fluxes and also depends on the definition of the generalized cross section, which is different in the literature (see, for example, [21] for a discussion). We will turn to the absolute values of the cross section (9) in Sec. V.

III. TWO-PHOTON GEOMETRICAL AND DYNAMICAL FACTORS

In order to proceed to the particular case of two-photon two-color single ionization, we first build the two-photon statistical tensors (see Appendix A) according to standard prescriptions [51]:

$$\rho^{2\gamma}_{k_\gamma q_\gamma}(\pi_1 L_1, \pi_2 L_2 : L_\gamma; \pi'_1 L'_1, \pi'_2 L'_2 : L'_\gamma) = \sum_{k_1 q_1 k_2 q_2} \hat{k}_1 \hat{k}_2 \hat{L}_\gamma \hat{L}'_\gamma (k_1 q_1, k_2 q_2 \,|\, k_\gamma q_\gamma) \begin{Bmatrix} L_1 & L_2 & L_\gamma \\ L'_1 & L'_2 & L'_\gamma \\ k_1 & k_2 & k_\gamma \end{Bmatrix} \times \rho_{k_1 q_1}(\pi_1 L_1; \pi'_1 L'_1)\rho_{k_2 q_2}(\pi_2 L_2; \pi'_2 L'_2). \tag{10}$$

The statistical tensors (10) obey the relation (5). Statistical tensors of a larger number of photons with different frequencies can be built in a similar way [50]. Statistical tensors of individual photons for arbitrary field multipoles in Eq. (10) are known. They have the simplest general form in the coordinate system $S_\parallel$ with the z axis along the photon beam [50,51,53]:

$$\rho^{\parallel}_{k0}(\pi L, \pi' L') = (-1)^{L'-1}\frac{\hat{L}\hat{L}'}{6}(L1, L'-1\,|\,k0) \times [1 + (-1)^f + p_3(1 - (-1)^f)], \tag{11}$$

$$\rho^{\parallel}_{k\pm 2}(\pi L, \pi' L') = (-1)^{L'+\pi'}\frac{\hat{L}\hat{L}'}{6}(L1, L'1\,|\,k2) \times (\pm 1)^f p_l \exp[\mp 2i\xi], \tag{12}$$

where $f = L + L' + \pi + \pi' - k$,

$$p_l = \sqrt{p_1^2 + p_2^2}, \quad \cos 2\xi = \frac{p_1}{p_l}, \quad \sin 2\xi = \frac{p_2}{p_l}. \tag{13}$$

The angle ξ indicates the principal axis of the polarization ellipse of the corresponding photon beam with respect to the x axis, which is fixed perpendicular to the photon beam. The Stokes parameters $p_1 = +1(-1)$ and $p_2 = +1(-1)$ describe radiation that is completely linearly polarized in the direction $\xi = 0$, x axis ($\xi = \frac{\pi}{2}$, y axis) and $\phi = \frac{\pi}{4}$ ($\phi = \frac{3\pi}{4}$), respectively, while p_l is the degree of linear polarization. The Stokes parameter $p_3 = +1(-1)$ corresponds to the positive (negative) value of the photon helicity. Statistical tensors $\rho^{\parallel}_{kq}(\pi L, \pi' L')$ with $q \neq 0, \pm 2$ vanish. A general factor in Eqs. (11) and (12) is chosen to yield the standard normalization $\rho_{00}(E1, E1) = \frac{1}{\sqrt{3}}$. The tensors (11) and (12) can be transformed to an arbitrary coordinate system S by rotation

$$\rho^{S}_{kq}(\pi L, \pi' L') = \sum_{q'} D^{k*}_{q' q}(R)\,\rho^{\parallel}_{kq'}(\pi L, \pi' L'), \tag{14}$$

where the Wigner D function is defined as in [52] and the rotation R transforms the frame $S_\parallel$ into the frame S. The statistical tensors (11) and (12) for $\{\pi L, \pi' L'\} = \{E1, E1\}, \{E1, E2\}, \{E1, M1\}$ in terms of the Stokes parameters are tabulated in [53]. Those tensors, which are

needed in the further derivations, are given in Appendix A, Eqs. (A4)–(A12).

The symmetry properties of the geometrical and dynamical factors are important in deriving the PADs. Permutation $\{\pi_1 L_1 \leftrightarrow \pi_2 L_2;\ \pi_1' L_1' \leftrightarrow \pi_2' L_2'\}$ in (10) leads to the relation

$$\rho^{2\gamma}_{k_\gamma q_\gamma}(\pi_1 L_1,\pi_2 L_2 : L_\gamma;\pi_1' L_1',\pi_2' L_2' : L_\gamma') = (-1)^\eta \rho^{2\gamma}_{k_\gamma q_\gamma}(\pi_2 L_2,\pi_1 L_1 : L_\gamma;\pi_2' L_2',\pi_1' L_1' : L_\gamma'), \quad (15)$$

where $\eta = L_1 + L_2 + L_\gamma + L_1' + L_2' + L_\gamma'$. A similar permutation symmetry is valid for the two-photon geometrical factors [see (4)]

$$F^{2\gamma}_{k_0 k k_\gamma}(\pi_1 L_1,\pi_2 L_2 : L_\gamma;\pi_1' L_1',\pi_2' L_2' : L_\gamma') = (-1)^\eta F^{2\gamma}_{k_0 k k_\gamma}(\pi_2 L_2,\pi_1 L_1 : L_\gamma;\pi_2' L_2',\pi_1' L_1' : L_\gamma'). \quad (16)$$

For fixed parities π_0 and π_f of the initial atomic and final ionic states, respectively, the two-photon transition matrix elements—due to the parity conservation in the photoionization process—obey the relationship

$$\langle \alpha_f J_f, \ell j : J \,||\, T \,||\, \alpha_0 J_0, \alpha_\gamma L_\gamma : J\rangle = (-1)^\nu \langle \alpha_f J_f, \ell j : J \,||\, T \,||\, \alpha_0 J_0, \alpha_\gamma L_\gamma : J\rangle, \quad (17)$$

where $\nu = \pi_1 + L_1 + \pi_2 + L_2 + \pi_0 + \pi_f + \ell$. Then it follows from Eq. (3)

$$B^{2\gamma}_{k_0 k k_\gamma}(\pi_1 L_1,\pi_2 L_2 : L_\gamma;\pi_1' L_1',\pi_2' L_2' : L_\gamma') = (-1)^{\nu'} B^{2\gamma}_{k_0 k k_\gamma}(\pi_1 L_1,\pi_2 L_2 : L_\gamma;\pi_1' L_1',\pi_2' L_2' : L_\gamma'), \quad (18)$$

where $\nu' = \pi_1 + \pi_2 + \pi_1' + \pi_2' + L_1 + L_2 + L_1' + L_2' + k$, restricting k to either even or odd values for a fixed set of the field multipoles.

IV. TWO PARALLEL RADIATION BEAMS

The equations of Secs. II and III allow us to write down the PAD for two-photon ionization under very general conditions. In this paper we restrict ourselves to the lowest-order nondipole corrections, when the interaction of one of the photons with the atom can be described within the electric dipole $E1$ approximation, while for the other photon accounting for the lowest-order nondipole corrections is needed. This is appropriate, for example, for pump-probe experiments with combined XUV or x-ray and optical laser beams. Furthermore, bearing in mind modern experimental facilities, we consider in this paper parallel radiation beams and unpolarized initial atomic states.

Using Eqs. (7), (8), and the permutation properties of the geometrical factors (16), the angular distribution (2) can be cast into the form

$$W(\vartheta,\varphi) = \sum_{k,L} B_k^{11}(LL) F_k^{11}(LL) + 2\,\mathrm{Re} \sum_{k,L>L'} B_k^{11}(LL') F_k^{11}(LL') + 4\,\mathrm{Re} \sum_{k,LL'} B_k^{12}(LL') F_k^{12}(LL'). \quad (19)$$

Here we assumed that the dominating nondipole effect in the PAD is caused by the $E1$-$E2$ interference of the multipole amplitudes. The $M1$ photoionization amplitude vanishes nonrelativistically. In Eq. (19) we abbreviated

$$F_k^{11}(LL') \equiv F^{2\gamma}_{0kk}(E1,E1 : L; E1,E1 : L'), \quad (20)$$

$$B_k^{11}(LL') \equiv B^{2\gamma}_{0kk}(E1,E1 : L; E1,E1 : L'), \quad (21)$$

$$F_k^{12}(LL') \equiv F^{2\gamma}_{0kk}(E1,E1 : L; E2,E1 : L') \equiv (-1)^{L+L'+1} F^{2\gamma}_{0kk}(E1,E1 : L; E1,E2 : L'), \quad (22)$$

$$B_k^{12}(LL') \equiv \tfrac{1}{2}\big[B^{2\gamma}_{0kk}(E1,E1 : L; E2,E1 : L') + (-1)^{L+L'+1} \times B^{2\gamma}_{0kk}(E1,E1 : L; E1,E2 : L')\big]. \quad (23)$$

According to Eqs. (7) and (8), $B_k^{11}(LL)$ and $F_k^{11}(LL)$ are real. The first two terms in Eq. (19) describe two-photon PAD in the pure electric dipole approximation, while the last term gives the first-order nondipole corrections. The values of k and L are restricted by triangular rules, in particular $|L - L'| \leqslant k \leqslant L + L'$. For initial atomic and final ionic states with definite parity, $k = 0,2,4$ in the first term of Eq. (19), $k = 2$ in the second term of Eq. (19), and $k = 1,3,5$ in the last term of Eq. (19). The last term in Eq. (19) vanishes when the photoelectron is emitted in the so-called "dipole plane," perpendicular to the photon beams. To show this, we choose the z axis along the photon beams. Then, for $k =$ odd and $\vartheta = \frac{\pi}{2}$, it follows from (6) that only terms with $q =$ odd give nonvanishing contributions to the PAD, because $Y_{kq}(\frac{\pi}{2},\varphi) = 0$ for $k + q =$ odd. However, the two-photon tensors (10) contributing to the first-order nondipole correction vanish for odd projections [see Eqs. (11) and (12)].

For stimulated emission by the optical photon, Eq. (19) remains valid with the geometrical and dynamical factors having a different meaning. This point will be considered in another publication.

Let us now specify Eq. (19) to particular cases.

A. Two circularly polarized radiation beams

For two circularly polarized radiation beams, Eq. (19) gives

$$W_{++}(\vartheta,\varphi) = \sum_{k=0}^{5} C_k^{++} P_k(\cos\vartheta), \quad (24)$$

$$W_{+-}(\vartheta,\varphi) = \sum_{k=0}^{5} C_k^{+-} P_k(\cos\vartheta), \quad (25)$$

where $++$ and $+-$ correspond to positive and negative helicities of the radiation beams, respectively, and the angle ϑ is counted from the propagation direction of the radiation beams. Note that $W_{++}(\vartheta,\varphi) = W_{--}(\vartheta,\varphi)$ and $W_{+-}(\vartheta,\varphi) = W_{-+}(\vartheta,\varphi)$. In Eqs. (24) and (25), terms with $k =$ even represent the dipole contributions originating from the pure $E1$ transitions, while terms with $k =$ odd are due to the first-order nondipole corrections. Explicit expressions for the coefficients C_k^{++} and C_k^{+-} in terms of dynamical factors (21) and (23) are given in Appendix B, Eqs. (B1)–(B10). For particular cases the coefficients in Eqs. (24) and (25) may be related, providing

simpler expressions for the PADs. An appropriate example will be given in Sec. V.

The PAD has axial symmetry with respect to the direction of the beams propagation (z axis). The forward-backward symmetry is violated due to the first-order nondipole corrections.

The circular dichroism in the photoelectron angular distribution (CDAD) takes the form

$$\begin{aligned}\mathrm{CDAD} &\equiv W_{++}(\vartheta,\varphi) - W_{+-}(\vartheta,\varphi)\\ &= \tfrac{1}{4}(C_0^{\Delta} + C_2^{\Delta} + 3C_2^{\Delta}\cos 2\vartheta)\\ &\quad + \tfrac{1}{4}(3C_1^{\Delta} + 3C_3^{\Delta} + 5C_3^{\Delta}\cos 2\vartheta)\cos\vartheta, \qquad (26)\end{aligned}$$

where $C_k^{\Delta} = C_k^{++} - C_k^{+-}$. Note that terms with the highest powers of cosine in Eqs. (24) and (25) are canceled in the CDAD (26).

B. One circularly polarized and one linearly polarized radiation beam

This case is realistic for experiments with linearly polarized XFEL radiation in combination with an optical laser whose polarization can be controlled easily. Equation (19) gives

$$\begin{aligned}W_{\pm}(\vartheta,\varphi) &= \sum_{k=0}^{5} C_k P_k(\cos\vartheta) + \cos 2\varphi \sum_{k=2}^{5} \bar{C}_k P_k^2(\cos\vartheta)\\ &\quad \pm \sin 2\varphi\big[C P_2^2(\cos\vartheta) + C' P_3^2(\cos\vartheta)\big]. \qquad (27)\end{aligned}$$

It is implied that the z axis is chosen along the photon beams and the x axis is chosen along the linear polarization. The signs, $+$ or $-$, indicate the helicity of the circularly polarized photon, $P_k^m(x)$ are the associated Legendre polynomials [54], and the coefficients C_k, $\bar{C}_k$, C, and C' are given in Appendix B, Eqs. (B11)–(B20). Similar to the previous case, terms with $k =$ even in Eq. (27) originate from pure dipole transitions, while terms with $k =$ odd are due to first-order nondipole corrections. The latter break down the symmetry with respect to the dipole xy plane.

The parametrization (27) is identical for the two cases: (a) for linearly polarized radiation the nondipole $E2$ transitions are taken into account, while the circularly polarized radiation is treated within the dipole approximation and (b) linearly polarized radiation is treated within the dipole approximation, while for the circularly polarized radiation the $E2$ transitions are included. Equation (27) for cases (a) and (b) differ only by the two nondipole coefficients, $\bar{C}_3$ and C' [see a note to Eqs. (B19) and (B20) in Appendix B].

The CDAD, which is the difference between the PADs for right (+) and left (−) polarized photons, follows from Eq. (27):

$$\begin{aligned}\mathrm{CDAD} &\equiv W_+ - W_-\\ &= 6\,\sin 2\varphi\,\sin^2\vartheta\,(C + 5C'\cos\vartheta). \qquad (28)\end{aligned}$$

In spite of the complicated expression for the PAD (27), the CDAD has a simple form with only two terms: one from the dipole part of the cross section and one from the first-order nondipole corrections. For fixed ϑ the CDAD reaches maximum absolute values at the angle $\varphi = \frac{\pi}{4}$. The dipole term of Eq. (28) shows the similar angle dependence as derived previously in [45] [see their Eq. (11)] for the CDAD in the two-photon two-color ionization of S states.

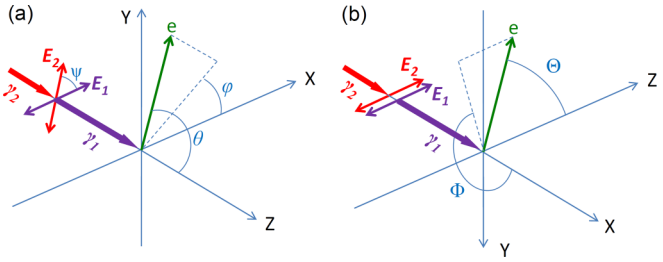

FIG. 1. (Color online) Geometry of the process with two collinear linearly polarized radiation beams: (a) general case with adjustable angle between the polarizations of the beams in the coordinate system $S^{\parallel}$; (b) for parallel polarizations of the beams in the alternative coordinate system $S^{\perp}$.

C. Two linearly polarized radiation beams

For linearly polarized beams the PAD depends on the adjustable angle $\psi = \xi_2 - \xi_1$ between the polarization directions of the photon beams [see Fig. 1(a)]. The PAD is obtained by Eq. (19), which is more convenient to transform into the frame with the z axis along the direction of polarization of one of the photons and the x axis along the beams. The conversion is performed by the relations

$$\cos\Theta = \sin\vartheta\cos\varphi, \quad \cot\Phi = -\frac{\cot\vartheta}{\sin\varphi}. \qquad (29)$$

The PAD can then be cast into the following form, where we explicitly allocated the angle dependencies:

$$\begin{aligned}&W_{\psi}(\Theta,\Phi)\\ &= \sum_{k=0,2,4}\big(C_k^s\sin^2\psi + C_k^c\cos^2\psi\big)P_k(\cos\Theta)\\ &\quad + \sin 2\psi\,\sin\Phi\sum_{k=2,4} C_k^1 P_k^1(\cos\Theta)\\ &\quad + \sin^2\psi\,\cos 2\Phi\sum_{k=2,4} C_k^2 P_k^2(\cos\Theta)\\ &\quad + \cos\Phi\sum_{k=1,3,5}\big(C_k^s\sin^2\psi + C_k^c\cos^2\psi\big)P_k^1(\cos\Theta)\\ &\quad + \sin 2\psi\,\sin 2\Phi\sum_{k=3,5} C_k^2 P_k^2(\cos\Theta)\\ &\quad + \sin^2\psi\,\cos 3\Phi\sum_{k=3,5} C_k^3 P_k^3(\cos\Theta). \qquad (30)\end{aligned}$$

The dynamical coefficients in Eq. (30) are given in Appendix B, Eqs. (B21)–(B34). The pure dipole part, represented by the first three sums in Eq. (30), is of the form found in [55,56]. The three last sums represent the first-order nondipole corrections.

Additional symmetries of the PAD appear for parallel and perpendicular directions of the polarizations. For the particular case of parallel polarizations [$\psi = 0$, Fig. 1(b)], we obtain from Eq. (30)

$$\begin{aligned}W_{0^\circ}(\Theta,\Phi) &= W_0\big[1 + \beta_2^{(2)}P_2(\cos\Theta) + \beta_4 P_4(\cos\Theta)\\ &\quad + (\delta^{(2)} + \gamma^{(2)}\cos^2\Theta + \gamma_4\cos^4\Theta)\sin\Theta\cos\Phi\big],\end{aligned} \qquad (31)$$

where $W_0 = C_0^c$, $\beta_2^{(2)} = (C_0^c)^{-1}C_2^c$, $\beta_4 = (C_0^c)^{-1}C_4^c$, $\delta^{(2)} = (C_0^c)^{-1}(C_1^c - \frac{3}{2}C_3^c + \frac{15}{8}C_5^c)$, $\gamma^{(2)} = \frac{15}{4}(C_0^c)^{-1}(2C_3^c - 7C_5^c)$, and $\gamma_4 = \frac{315}{8}(C_0^c)^{-1}C_5^c$. The superscript $^{(2)}$ distinguishes the parameters $\beta_2^{(2)}$, $\delta^{(2)}$, and $\gamma^{(2)}$ from the corresponding ones in the well-known PAD in single-photon ionization, accounting for the first-order nondipole corrections [16]

$$\frac{d\sigma}{d\Omega} = \frac{\sigma_{E1}}{4\pi}[1 + \beta P_2(\cos\Theta) + (\delta + \gamma\,\cos^2\Theta)\sin\Theta\,\cos\Phi]. \tag{32}$$

In Eq. (32), σ_{E1} is the total photoionization cross section in the dipole approximation, β is the asymmetry parameter, and γ, δ are the nondipole asymmetry parameters. The first three terms in Eq. (31) yield the well-known PAD in two-photon ionization in the dipole approximation. The next two terms are similar to the PAD (32) in single-photon ionization, except that the parameters $\delta^{(2)}$ and $\gamma^{(2)}$ are now expressed in terms of the two-photon amplitudes. The term with the dynamical coefficient γ_4 in Eq. (31) is characteristic for the PAD in the two-photon ionization with the lowest-order nondipole corrections. It is absent in the case of single-photon ionization.

Simpler expressions are obtained for linear dichroism in the photoelectron angular distribution (LDAD), which is defined as $\mathrm{LDAD}(\psi/\psi + \frac{\pi}{2}) = W_\psi(\vartheta,\varphi) - W_{\psi+\frac{\pi}{2}}(\vartheta,\varphi)$. For example, as follows from Eq. (30),

$$\mathrm{LDAD}\left(\frac{\pi}{4}\Big/\frac{3\pi}{4}\right) = 2\,\sin\Phi\left[\sum_{k=2,4} C_k^1 P_k^1(\cos\Theta) + 2\,\cos\Phi\sum_{k=3,5} C_k^2 P_k^2(\cos\Theta)\right]. \tag{33}$$

D. Angle-integrated cross section

Integrating Eq. (19) over the angles of the electron emission gives the integral generalized cross section [see Eq. (9)]

$$\begin{aligned}\sigma = c\frac{4\pi}{\hat{J}_0}\frac{1}{12\sqrt{5}}\{&[2\sqrt{5}B_0^{11}(00) + \sqrt{15}B_0^{11}(11) + 7B_0^{11}(22)] \\ &+ p_3^{(1)}p_3^{(2)}[5B_0^{11}(22) - \sqrt{15}B_0^{11}(11) - 2\sqrt{5}B_0^{11}(00)] \\ &+ p_l^{(1)}p_l^{(2)}\cos 2\psi\,[B_0^{11}(22) - \sqrt{15}B_0^{11}(11) \\ &+ 2\sqrt{5}B_0^{11}(00)]\}.\end{aligned} \tag{34}$$

Thus the angle-integrated two-photon ionization cross section is not sensitive to the first-order nondipole corrections, regardless of the polarization state of the photons. Measurements collecting photoelectrons in the 4π geometry, such as experiments with a magnetic bottle [41,57], are sensitive to the nondipole contribution only in the next order. The particular cases of Eq. (34) are equivalent to those used in the XUV + optical laser pump-probe studies of the two-photon ionization with observing the angular dependence of the intensities, for example [40,42]. Note that in the limiting cases of both right (left) circularly polarized photons ($p_3^{(1)}p_3^{(2)} = 1$, $p_\ell^{(1)}p_\ell^{(2)} = 0$) and parallel linearly polarized photons ($p_3^{(1)}p_3^{(2)} = 0$, $p_l^{(1)}p_l^{(2)}\cos 2\psi = 1$), the maximum ratio of the cross sections for circular and linear polarized beams given by Eq. (34) is $\frac{3}{2}$, in accordance with [58,59]. Here we obtained this result for arbitrary angular momentum J_0 of an initially unpolarized atomic state.

Equation (34) shows that the angle-integrated dichroism vanishes in the case of one circularly polarized and one linearly polarized radiation beam ($p_l^{(1)}p_l^{(2)} = p_3^{(1)}p_3^{(2)} = 0$). Furthermore, for two linearly polarized beams the angle-integrated linear dichroism $\mathrm{LD}(\frac{\pi}{4}/\frac{3\pi}{4})$ also vanishes ($p_3^{(1)}p_3^{(2)} = p_l^{(1)}p_l^{(2)}\cos 2\psi = 0$).

V. *K*-SHELL TWO-PHOTON TWO-COLOR IONIZATION OF Ne

As a numerical example of applying the developed formalism, we take the ATI of the $1s$ subshell of Ne, when the two-photon ionization proceeds by absorption of the XUV photon and the optical photon (Fig. 2). Noticeable nondipole effects in the PAD in single-photon $1s$ ionization of Ne have been predicted [60]. It is natural to expect that the nondipole effects should show up in the two-photon two-color ionization as well, if the energy of the XUV photon is in the same energy range. We assume that the interaction of the optical photon with the atom can be described in the dipole approximation, i.e., the nondipole contribution comes from the XUV photon. We fix the energy of the optical photon in the infrared (IR) at 1.5 eV and limit the energies of the photons to 3 keV, so that an energy resolution of an electron spectrometer of 10^{-3}–10^{-4} still allows one to resolve the ATI photoelectron line from the main photoelectron line. Based on calculations [60] for the Ne($1s^{-1}$) photoelectron line, we expect the second-order nondipole effects to be small at these photon energies.

We assume that the two-photon ionization is dominated by the process, in which the $1s$ electron first absorbs the XUV photon (solid arrows in Fig. 2). The two-photon transition matrix element in second-order perturbation theory then takes the form

$$\begin{aligned}&\langle\alpha_f J_f, \ell j : J \,||\, T \,||\, \alpha_0 J_0, (\pi_1 L_1 E1) L_\gamma : J\rangle \\ &\quad = \langle\alpha_f J_f, \ell j : J \,||\, \{T^{\pi_1 L_1} \otimes T^{E1}\}_{L_\gamma} \,||\, \alpha_0 J_0\rangle\end{aligned}$$

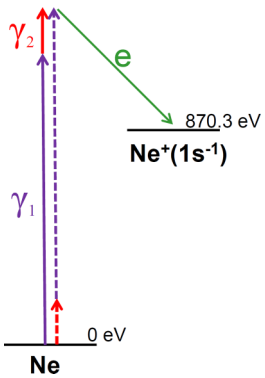

FIG. 2. (Color online) Scheme of the two-photon two-color ATI of the Ne atom from the $1s$ shell (see text).

$$= (-1)^{1+L_1-J}\delta_{JL_\gamma}\hat{L}_1^{-1} \times \sum_\nu\!\!\!\!\!\!\int \delta_{J_\nu L_1}\frac{\langle \alpha_f J_f,\ell j : J \,||\, T^{E1} \,||\, \nu\rangle\langle \nu \,||\, T^{\pi_1 L_1} \,||\, 0\rangle}{E_\nu - E_0 - \omega_1}, \quad (35)$$

where $\pi_1 L_1 = E1$ or $E2$ with the electric dipole and electric quadrupole transition operators in the nonrelativistic long-wave approximation

$$T_\mu^{E1} = \sqrt{\frac{4\pi}{3}}\sum_p r_p Y_{1\mu}(\theta_p,\phi_p), \quad (36)$$

$$T_\mu^{E2} = \frac{i\alpha\omega}{2\sqrt{3}}\sqrt{\frac{4\pi}{5}}\sum_p r_p^2 Y_{2\mu}(\theta_p,\phi_p). \quad (37)$$

Here we introduced the tensorial product of two reduced tensor operators [52]. The summations in Eqs. (36) and (37) are taken over the atomic electrons and μ denotes the cyclic projection of the operators. Furthermore, with the transition matrix element (35), the second term in Eq. (23) for the dynamical factors vanishes. Using standard methods of Racah algebra, Eq. (35) can be reduced within the framework of a single-particle model and the LS-coupling approximation. Substituting the result into Eq. (3) with $J_0 = 0$ and performing the summations, we finally obtain for the dynamical factors of Eq. (19)

$$B_k^{11}(LL') = 6\hat{k}^{-1}(L0,L'0\,|\,k0)(10,10\,|\,L0) \times (10,10\,|\,L'0)D_L D_{L'}^*, \quad (38)$$

$$B_k^{12}(LL') = -3\hat{k}^{-1}(L0,L'0\,|\,k0)(10,10\,|\,L0) \times (20,10\,|\,L'0)D_L Q_{L'}^*, \quad (39)$$

where

$$D_L = \sum_{\varepsilon'}\!\!\!\!\!\!\int \frac{d_{1s\to\varepsilon' p}d_{\varepsilon' p\to\varepsilon L}}{\varepsilon' - E_{1s} - \omega_1}, \quad (40)$$

$$Q_L = \sum_{\varepsilon'}\!\!\!\!\!\!\int \frac{q_{1s\to\varepsilon' d}d_{\varepsilon' d\to\varepsilon L}}{\varepsilon' - E_{1s} - \omega_1}, \quad (41)$$

$$d_{a\to b} = \int_0^\infty P_b^*(r)P_a(r)r\,dr, \quad (42)$$

$$q_{a\to b} = \frac{i\alpha\omega}{2\sqrt{3}}\int_0^\infty P_b^*(r)P_a(r)r^2\,dr. \quad (43)$$

Here $P_a(r)$ and $P_b(r)$ are the radial electron wave functions in the states a and b, respectively. The dipole integrals (42) with two continuum states were calculated according to the recipes developed in [61,62].

The $1s$ electron wave function was obtained in the Hartree-Fock approximation for the ground state of Ne [63]. The atomic wave functions were then fixed to obtain the continuum electron orbitals $P_{\varepsilon\ell}(r)$ in the Ne($1s^{-1}$) frozen-core Hartree-Fock approximation. The continuum wave functions are normalized asymptotically according to

$$\lim_{r\to\infty} P_{\varepsilon\ell}(r) = i^\ell e^{-i\delta_\ell(\varepsilon)}\sqrt{\frac{2}{\pi p}} \times \sin\left(pr + \frac{1}{p}\ln 2pr - \frac{\pi\ell}{2} + \delta_\ell(\varepsilon)\right), \quad (44)$$

where $\delta_\ell(\varepsilon)$ is the scattering phase. With this normalization, the coefficient c in Eq. (34) is $2\pi^2\alpha^2\omega_1\omega_2/3$ to yield the generalized cross section in atomic units (1.897×10^{-50} cm^{4}s). Our model gives the nondipole asymmetry parameters for the main photoelectron line in agreement with the relativistic independent-particle approximation of [60] (see the parameter γ in Fig. 3).

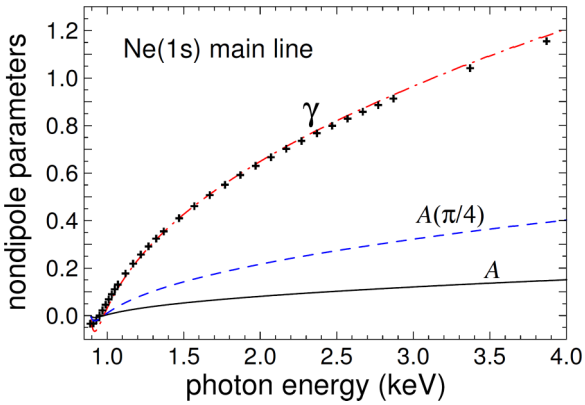

FIG. 3. (Color online) Nondipole parameters for the main Ne($1s^{-1}$) photoelectron line. Chain red: nondipole asymmetry parameter γ, Eq. (32). Dashed blue: differential forward-backward asymmetry at the angle $\frac{\pi}{4}$ to the quantization axis; $A(\frac{\pi}{4}) = \gamma/3$ is independent of the photon polarization. Solid black: integral forward-backward asymmetry; $A = \gamma/8$ is independent of the photon polarization. Crosses: relativistic independent-particle approximation [60] for γ.

It can be seen from Eqs. (38) and (39) explicitly that the dynamical coefficients with similar sets of L, L' but different k are related by a simple algebraic factor. Furthermore, $L = 0,2$ and $L' = 0,2$ in (38), $L = 0,2$ and $L' = 1,3$ in (39), and $L +$

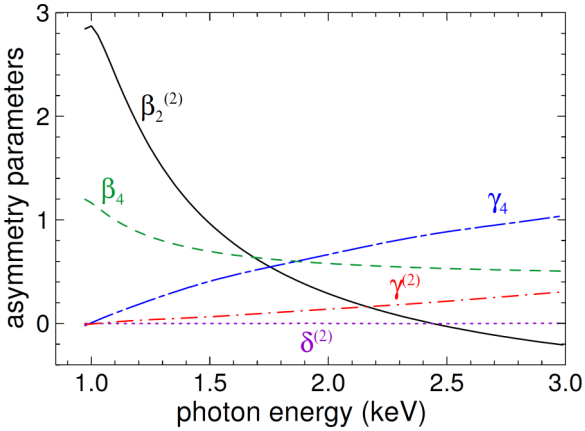

FIG. 4. (Color online) Angular asymmetry parameters of Eq. (31) for the two-photon two-color Ne($1s$) ATI by linearly polarized photons (see text).

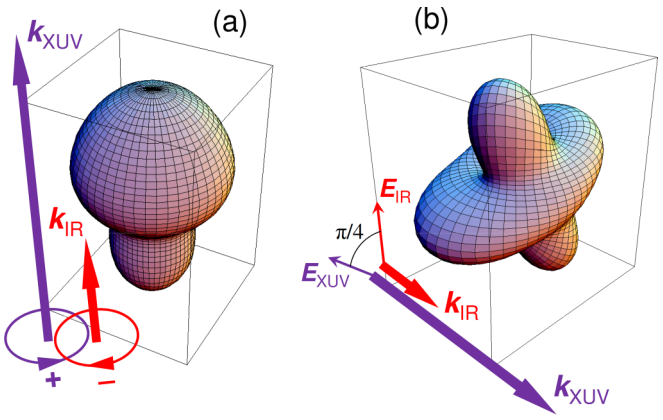

FIG. 5. (Color online) 3D photoelectron angular distributions in the Ne(1s) ATI at the XUV photon energy of 3 keV: (a) ionization by two circularly polarized photon beams with opposite helicities; (b) ionization by two linearly polarized photon beams with the angle $\frac{\pi}{4}$ between their electric-field vectors $\boldsymbol{E}_{\rm XUV}$ and $\boldsymbol{E}_{\rm IR}$. The wave vectors of the XUV ($\boldsymbol{k}_{\rm XUV}$) and IR ($\boldsymbol{k}_{\rm IR}$) radiation beams are shown.

$L' + k =$ even. As a result, the general equations of Sec. IV are simplified. For example, Eq. (24) for two circularly polarized beams with equal helicities transforms into

$$W_{++}(\vartheta,\varphi) = \frac{3}{2}|D_d|^2 \sin^4\vartheta\left(1 + 3\sqrt{5}\frac{\mathrm{Re}(D_d Q_f^*)}{|D_d|^2}\cos\vartheta\right). \tag{45}$$

Here the nondipole contribution is given by the term containing the cosine. In the dipole limit Eq. (45) reproduces the well-known $\sin^4\vartheta$ dependence for two-photon ionization from an S state by circularly polarized light [58].

As another example, for two linearly polarized beams in the dipole approximation, the terms with $k =$ even in Eq. (30) coincide with Eqs. (2) and (6) of [56] for the PADs in photoionization of the ^1P laser-excited states of the alkaline-earth metals, provided depolarization due to hyperfine structure [56] is neglected.

Figure 4 displays the asymmetry parameters in the PAD (31) for two beams with parallel linear polarizations. At XUV photon energies near 2 keV, the two-photon two-color nondipole and dipole asymmetry parameters, γ_4 and β_4, respectively, become approximately equal, with γ_4 exceeding β_4 with increasing the photon energy. This points to large nondipole effects in the PADs. It is illustrated in Fig. 5, which shows the PADs for the photon energy of 3 keV deviating considerably from the shape inherent to the dipole approximation. In particular, the symmetry with respect to the dipole plane perpendicular to the radiation beams ($\vartheta = \frac{\pi}{2}$) is strongly violated. The latter is better seen in Fig. 6, where meridional cuts of the PADs are displayed for three combinations of the XUV and IR photon beam polarization. The nondipole corrections lead to preferential electron emission into the forward hemisphere, except for the case ($\varphi = \frac{\pi}{2}$) in panel (b). For the latter geometry the nondipole terms vanish, which is specific for ionization from the S states. In the deep minimas of the cross sections, and especially at the angles of photoemission where the PADs in the dipole approximation drops to zero, one should incorporate additional effects into the model, such as relativistic splitting of the electron orbitals in the continuum and the second-order nondipole corrections.

We concentrate now on the differential forward-backward asymmetry

$$A(\vartheta,\varphi) = \frac{W(\vartheta,\varphi) - W(\pi - \vartheta,\varphi)}{W(\vartheta,\varphi) + W(\pi - \vartheta,\varphi)} \tag{46}$$

and the integral forward-backward asymmetry

$$A = \frac{\int_{\Omega+} W(\vartheta,\varphi)\,d\Omega - \int_{\Omega-} W(\vartheta,\varphi)d\Omega}{\int W(\vartheta,\varphi)d\Omega}, \tag{47}$$

where $\Omega+$ ($\Omega-$) represents the forward (backward) hemisphere. The forward-backward asymmetry is a convenient quantity to study the nondipole effects, since it vanishes in the dipole approximation.

Figure 7 exhibits selected results for the forward-backward differential and integral asymmetries for various polarizations of the incoming XUV and IR radiation beams. For comparison, integral and differential forward-backward asymmetries of the main photoelectron line are shown in Fig. 3. The values of the forward-backward asymmetry generally increase monotonically with the XUV photon energy, except in the case of one circular and one linear polarized radiation beam [Fig. 7(b)]. This case is distinguished because the imaginary parts of the dynamical coefficients (38), (39) also contribute to the forward-backward asymmetries, in contrast to the other two cases with both linearly and both circularly polarized beams. Comparing the integral forward-backward asymmetry A of

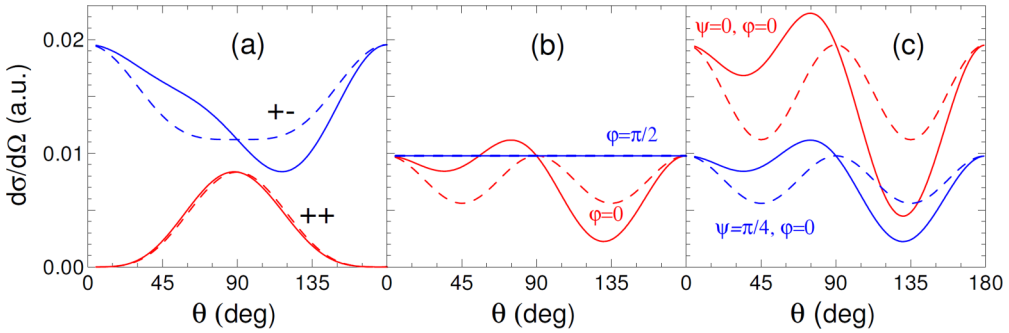

FIG. 6. (Color online) Same as in Fig. 5 on the absolute scale: (a) for two circularly polarized photon beams; (b) for linearly polarized XUV and circularly polarized IR photon beams; (c) for two linearly polarized photon beams. Solid: including the first-order nondipole corrections; dashed: pure dipole approximation.

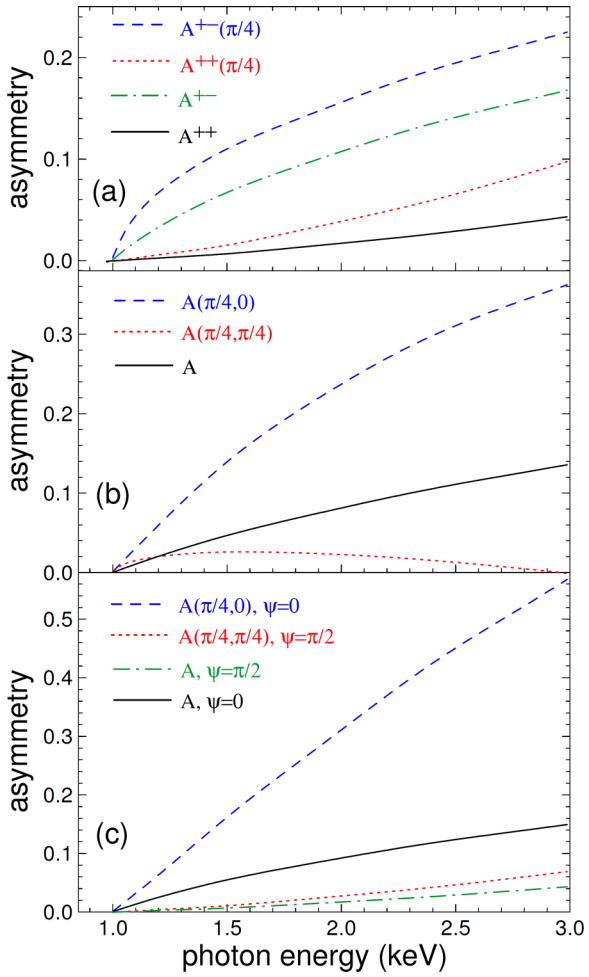

FIG. 7. (Color online) Forward-backward differential asymmetries $A(\vartheta,\varphi)$, Eq. (46), and integral asymmetries A, Eq. (47), for circularly polarized XUV and IR photons (a), linearly polarized XUV photon and circularly polarized IR photon (b), and linearly polarized XUV and IR photons (c).

the main photoelectron line (Fig. 3) with the corresponding asymmetry of the ATI line, A, $\psi = 0$ [Fig. 7(c)], we see that the forward-backward asymmetry in the latter case is slightly larger. One can find conditions for which the differential forward-backward asymmetry of the ATI line is much larger than the asymmetry of the main photoelectron line; see $A(\frac{\pi}{4},0)$, $\psi = 0$ in Fig. 7(c). Interestingly, the forward-backward asymmetry (46) in the direction of the beam propagation takes the form

$$A(\vartheta = 0,\varphi) = \frac{6}{\sqrt{5}} \frac{2\,\mathrm{Re}[(D_s - D_d)(Q_p^\star - Q_f^\star)]}{|D_s - D_d|^2}, \qquad (48)$$

independent of the polarization state of the photon beams. This "universal" forward-backward differential asymmetry (not shown) in our case is less than 0.02 over the entire range of photon energies considered.

The predicted values of the cross sections and the forward-backward asymmetries of the ATI line point to the possibility of observing nondipole effects by combining XUV free-electron and optical laser radiation beams.

VI. CONCLUSIONS

The angular distribution of photoelectrons in two-photon two-color above-threshold atomic ionization was studied theoretically by accounting for the full multipole expansion of the radiation field and emphasizing independently variable polarizations of the radiation beams. The general formalism was applied to the analysis of first-order nondipole corrections for the experimentally most feasible arrangement with collinear photon beams. The derived expressions can be used to parametrize the photoelectron angular distributions and different kinds of dichroism. Calculations for the above-threshold (XUV + IR) $1s$ photoionization of Ne within the second-order perturbation theory predict large nondipole effects in the photoelectron angular distribution. These nondipole effects can be enhanced by selecting a suitable experimental geometry. In particular, the forward-backward asymmetry may be much larger than in the main photoelectron line. The predicted nondipole effects in two-photon two-color above-threshold ionization are measurable by combining XUV free-electron and optical laser radiation beams.

ACKNOWLEDGMENTS

The authors acknowledge support by the Russian Foundation for Basic Research (RFBR) under Grant No. 12-02-01123. E.V.G. gratefully acknowledges financial support by the Russian President Grant No. MK-6509.2012.2 and by the Dynasty Foundation via the Support Program for Young Scientists. This work is part of the project "Correlation and Polarization Phenomena in Ionization of Dilute Species by XUV and x-ray Radiation" in the framework of the German-Russian collaboration "Development and Use of Accelerator-Based Photon Sources." The authors are grateful to Klaus Bartschat for careful reading of the manuscript and suggestions for further improvement.

APPENDIX A: STATISTICAL TENSORS OF TWO PHOTONS

To derive Eq. (10) we consider the density matrix of two photons with fixed frequencies ω_1 and ω_2 in the laboratory system represented by their individual angular momenta L_1 and L_2, with projections M_1 and M_2 on the z axis, and parities π_1 and π_2. Since, according to our assumptions, the photons in the two beams are not correlated, the density matrix of the two absorbed photons is a product of the two density matrices, $\hat\rho = \hat\rho^{(1)}\hat\rho^{(2)}$, with zero matrix elements coupling the photons from the different beams. The superscripts $^{(1)}$ and $^{(2)}$ denote the "first" and "second" radiation beams, respectively. Furthermore, we assume that the polarization states of the photons are independent of their frequencies. Then we can write

$$\begin{aligned}
&\langle \omega_1\pi_1 L_1 M_1, \omega_2\pi_2 L_2 M_2 \,|\, \hat\rho \,|\, \omega_1\pi_1' L_1' M_1', \omega_2\pi_2' L_2' M_2'\rangle \\
&\quad = I^{(1)}(\omega_1) I^{(2)}(\omega_2) \langle \pi_1 L_1 M_1 \,|\, \hat\rho^{(1)} \,|\, \pi_1' L_1' M_1'\rangle \\
&\qquad \times \langle \pi_2 L_2 M_2 \,|\, \hat\rho^{(2)} \,|\, \pi_2' L_2' M_2'\rangle \\
&\qquad + I^{(1)}(\omega_2) I^{(2)}(\omega_1) \langle \pi_2 L_2 M_2 \,|\, \hat\rho^{(1)} \,|\, \pi_2' L_2' M_2'\rangle \\
&\qquad \times \langle \pi_1 L_1 M_1 \,|\, \hat\rho^{(2)} \,|\, \pi_1' L_1' M_1'\rangle, \qquad (A1)
\end{aligned}$$

where the boson symmetry of the basis two-photon bra and ket states on the left side of Eq. (A1) is taken into account and $I^{(i)}(\omega_j)$ $(i = 1,2,\ j = 1,2)$ is a factor that depends on the photon flux in the corresponding beam. In our case of different colors of the beams ($\omega_1 \neq \omega_2$), one of the two terms in Eq. (A1) vanishes. The overall normalization factor of the density matrix is a matter of convention; it does not affect the PADs and will be included in the factor c in Eq. (9). Using the definition of the statistical tensor

$$\rho_{kq}(\pi_1 L_1,\pi_2 L_2 : L;\pi_1' L_1',\pi_2' L_2' : L') = \sum_{MM'} (-1)^{L'-M'}(LM,L'-M' \mid kq) \times \langle \pi_1 L_1,\pi_2 L_2 : LM \mid \hat{\rho} \mid \pi_1' L_1',\pi_2' L_2' : L'M' \rangle, \quad \text{(A2)}$$

decoupling angular momenta of the two photons in the density matrix at the right side of (A2), accounting for Eq. (A1), transforming from the density matrices of the individual photons to their statistical tensors by the equation

$$\langle \pi LM \mid \hat{\rho} \mid \pi' L'M' \rangle = \sum_{kq} (-1)^{L'-M'}(LM,L'-M' \mid kq)\rho_{kq}(\pi L;\pi' L'), \quad \text{(A3)}$$

and performing summations over magnetic quantum numbers, we obtain Eq. (10). The first nonvanishing tensors of the photon in the coordinate system $S_\parallel$ [see Eqs. (11) and (12)] are

$$\rho^{\parallel}_{00}(E1,E1) = \frac{1}{\sqrt{3}}, \quad \text{(A4)}$$

$$\rho^{\parallel}_{10}(E1,E1) = \frac{1}{\sqrt{2}} p_3, \quad \text{(A5)}$$

$$\rho^{\parallel}_{20}(E1,E1) = \frac{1}{\sqrt{6}}, \quad \text{(A6)}$$

$$\rho^{\parallel}_{2\pm2}(E1,E1) = -\frac{1}{2} p_l \exp[\mp 2i\xi], \quad \text{(A7)}$$

$$\rho^{\parallel}_{10}(E1,E2) = -\frac{1}{\sqrt{2}}, \quad \text{(A8)}$$

$$\rho^{\parallel}_{20}(E1,E2) = -\sqrt{\frac{5}{6}} p_3, \quad \text{(A9)}$$

$$\rho^{\parallel}_{30}(E1,E2) = -\frac{1}{\sqrt{3}}, \quad \text{(A10)}$$

$$\rho^{\parallel}_{2\pm2}(E1,E2) = \pm\frac{\sqrt{5}}{6} p_l \exp[\mp 2i\xi], \quad \text{(A11)}$$

$$\rho^{\parallel}_{3\pm2}(E1,E2) = \frac{\sqrt{5}}{3\sqrt{2}} p_l \exp[\mp 2i\xi]. \quad \text{(A12)}$$

APPENDIX B: DYNAMICAL COEFFICIENTS IN THE ANGULAR DISTRIBUTION OF PHOTOELECTRONS

Below the coefficients in the expressions for the PAD are given in terms of the dynamical factors (21) and (23). For two circularly polarized radiation beams, Eqs. (24) and (25),

$$C_0^{++} = \frac{1}{\sqrt{5}} B_0^{11}(22), \quad \text{(B1)}$$

$$C_0^{+-} = \frac{1}{6\sqrt{5}}\left[2\sqrt{5}B_0^{11}(00) + \sqrt{15}B_0^{11}(11) + B_0^{11}(22)\right], \quad \text{(B2)}$$

$$C_2^{++} = \sqrt{\frac{10}{7}} B_2^{11}(22), \quad \text{(B3)}$$

$$C_2^{+-} = \frac{1}{3}\sqrt{\frac{5}{14}}\left[2\sqrt{7}\,\mathrm{Re}B_2^{11}(20) - \sqrt{21}B_2^{11}(11) - B_2^{11}(22)\right], \quad \text{(B4)}$$

$$C_4^{++} = C_4^{+-} = \frac{3}{\sqrt{70}} B_4^{11}(22), \quad \text{(B5)}$$

$$C_1^{++} = -4\sqrt{\frac{2}{21}}\mathrm{Re}\left[\sqrt{7}B_1^{12}(22) + \sqrt{5}B_1^{12}(23)\right], \quad \text{(B6)}$$

$$C_1^{+-} = -2\sqrt{\frac{2}{35}}\mathrm{Re}\left[\sqrt{35}B_1^{12}(01) - \sqrt{7}B_1^{12}(21) + \sqrt{35}B_1^{12}(12) + \sqrt{3}B_1^{12}(23)\right], \quad \text{(B7)}$$

$$C_3^{++} = -\frac{2}{3}\sqrt{\frac{14}{3}}\mathrm{Re}\left[\sqrt{3}B_3^{12}(22) + 2\sqrt{5}B_3^{12}(23)\right], \quad \text{(B8)}$$

$$C_3^{+-} = -\frac{2}{3}\sqrt{\frac{7}{15}}\mathrm{Re}\left[2\sqrt{15}B_3^{12}(03) - 3\sqrt{15}B_3^{12}(12) + 3\sqrt{3}B_3^{12}(21) - 2\sqrt{2}B_3^{12}(23)\right], \quad \text{(B9)}$$

$$C_5^{++} = C_5^{+-} = -\frac{4}{3}\sqrt{\frac{55}{21}}\mathrm{Re}B_5^{12}(23). \quad \text{(B10)}$$

For one linearly and one circularly polarized photon beam, Eqs. (27) and (28),

$$C_0 = \frac{1}{12\sqrt{5}}\left[2\sqrt{5}B_0^{11}(00) + \sqrt{15}B_0^{11}(11) + 7B_0^{11}(22)\right], \quad \text{(B11)}$$

$$C_2 = \frac{1}{6}\sqrt{\frac{5}{14}}\left[2\sqrt{7}\,\mathrm{Re}B_2^{11}(20) - \sqrt{21}B_2^{11}(11) + 5B_2^{11}(22)\right], \quad \text{(B12)}$$

$$C_4 = -12\bar{C}_4 = \frac{3}{\sqrt{70}} B_4^{11}(22), \quad \text{(B13)}$$

$$\bar{C}_2 = -\frac{1}{6}\sqrt{\frac{5}{14}}\left\{\sqrt{7}\left[\mathrm{Re}B_2^{11}(20) - B_2^{11}(21)\right] + B_2^{11}(22)\right\}, \quad \text{(B14)}$$

$$C = \frac{1}{6}\sqrt{\frac{5}{2}}\mathrm{Im}\left[B_2^{11}(20) - B_2^{11}(21)\right], \quad \text{(B15)}$$

$$C_1 = -\sqrt{\frac{2}{105}}\mathrm{Re}\{\sqrt{105}[B_1^{12}(01)+B_1^{12}(12)] - \sqrt{21}B_1^{12}(21)+2\sqrt{35}B_1^{12}(22)+13B_1^{12}(23)\}, \quad \text{(B16)}$$

$$C_3 = -\frac{1}{3}\sqrt{\frac{7}{15}}\mathrm{Re}[2\sqrt{15}B_3^{12}(03)-3\sqrt{15}B_3^{12}(12) + 3\sqrt{3}B_3^{12}(21)+\sqrt{30}B_3^{12}(22)+8\sqrt{2}B_3^{12}(23)], \quad \text{(B17)}$$

$$C_5 = -20\bar{C}_5 = -\frac{4}{3}\sqrt{\frac{55}{21}}\mathrm{Re}B_5^{12}(23), \quad \text{(B18)}$$

$$\bar{C}_3 = \frac{1}{18}\sqrt{\frac{7}{5}}\mathrm{Re}[2\sqrt{5}B_3^{12}(03)+3B_3^{12}(21)-\sqrt{5}B_3^{12}(12) + 2\sqrt{10}B_3^{12}(22)+\sqrt{6}B_3^{12}(23)-\sqrt{10}B_3^{12}(13)], \quad \text{(B19)}$$

$$C' = \frac{1}{18}\sqrt{\frac{7}{5}}\mathrm{Im}[2\sqrt{5}B_3^{12}(03)-\sqrt{5}B_3^{12}(12)-\sqrt{10}B_3^{12}(13) - 3B_3^{12}(21)-\sqrt{10}B_3^{12}(22)-\sqrt{6}B_3^{12}(23)]. \quad \text{(B20)}$$

Equations (B19) and (B20) are given for case (a); see Sec. IV B. For case (b), the numerical coefficients at $B_3^{12}(12)$, $B_3^{12}(13)$, and $B_3^{12}(22)$ in Eqs. (B19) and (B20) change sign and, furthermore, the coefficient at $B_3^{12}(22)$ decreases and increases by a factor of 2, respectively.

For two linearly polarized photon beams, Eq. (30),

$$C_0^s = \frac{1}{2\sqrt{15}}[\sqrt{5}B_0^{11}(11)+\sqrt{3}B_0^{11}(22)], \quad \text{(B21)}$$

$$C_0^c = \frac{1}{3\sqrt{5}}[\sqrt{5}B_0^{11}(00)+2B_0^{11}(22)], \quad \text{(B22)}$$

$$C_2^s = -\frac{1}{2}\sqrt{\frac{5}{42}}[\sqrt{3}B_2^{11}(22)-\sqrt{7}B_2^{11}(11)+2\sqrt{21}\mathrm{Re}B_2^{11}(21)], \quad \text{(B23)}$$

$$C_2^2 = \frac{1}{12}\sqrt{\frac{5}{14}}[3B_2^{11}(22)-\sqrt{21}B_2^{11}(11)-2\sqrt{7}\mathrm{Re}B_2^{11}(21)], \quad \text{(B24)}$$

$$C_2^c = -\frac{4}{3}\sqrt{\frac{5}{14}}[\sqrt{7}\mathrm{Re}B_2^{11}(20)+B_2^{11}(22)], \quad \text{(B25)}$$

$$C_2^1 = \frac{1}{3}\sqrt{\frac{5}{14}}\{\sqrt{7}\mathrm{Re}[B_2^{11}(20)-B_2^{11}(21)]+B_2^{11}(22)\}, \quad \text{(B26)}$$

$$C_4^s = -\frac{1}{2}C_4^c = 2C_4^1 = 12C_4^2 = -\frac{6}{\sqrt{70}}B_4^{11}(22), \quad \text{(B27)}$$

$$C_1^s = -2\sqrt{\frac{2}{21}}\mathrm{Re}[\sqrt{7}B_1^{12}(22)+\sqrt{5}B_1^{12}(23)+\sqrt{21}B_1^{12}(12)], \quad \text{(B28)}$$

$$C_1^c = 2\sqrt{\frac{2}{105}}\mathrm{Re}[-\sqrt{105}B_1^{12}(01)+\sqrt{21}B_1^{12}(21) - \sqrt{35}B_1^{12}(22)-8B_1^{12}(23)], \quad \text{(B29)}$$

$$C_3^3 = \frac{1}{18}\sqrt{\frac{7}{6}}\mathrm{Re}[\sqrt{3}B_3^{12}(22)-\sqrt{5}B_3^{12}(23)+\sqrt{6}B_3^{12}(12) - \sqrt{3}B_3^{12}(13)], \quad \text{(B30)}$$

$$C_3^s = \frac{1}{9}\sqrt{\frac{7}{2}}\mathrm{Re}[9B_3^{12}(22)+\sqrt{15}B_3^{12}(23)-7\sqrt{2}B_3^{12}(12) - 5B_3^{12}(13)], \quad \text{(B31)}$$

$$C_3^c = \frac{4}{9}\sqrt{\frac{7}{10}}\mathrm{Re}[\sqrt{5}B_3^{12}(22)+2\sqrt{3}B_3^{12}(23)+3\sqrt{2}B_3^{12}(21) + 2\sqrt{10}B_3^{12}(03)], \quad \text{(B32)}$$

$$C_3^2 = \frac{1}{18}\sqrt{\frac{7}{5}}\mathrm{Re}[\sqrt{10}B_3^{12}(22)-\sqrt{6}B_3^{12}(23)-3B_3^{12}(21) - 2\sqrt{5}B_3^{12}(03)-\sqrt{5}B_3^{12}(12)-\sqrt{10}B_3^{12}(13)], \quad \text{(B33)}$$

$$C_5^s = -\frac{1}{4}C_5^c = 2C_5^2 = 12C_5^3 = \frac{4}{3}\sqrt{\frac{11}{105}}\mathrm{Re}B_5^{12}(23). \quad \text{(B34)}$$

[1] N. B. Delone and V. P. Krainov, *Atoms in Strong Light Fields* (Springer-Verlag, Berlin, 1985).

[2] F. H. M. Faisal, *Theory of Multiphoton Processes* (Plenum Press, New York, London, 1986).

[3] M. H. Mittleman, *Introduction to the Theory of Laser-Atom Interactions* (Plenum Press, New York and London, 1993).

[4] P. Lambropoulos, P. Maragakis, and J. Zhang, Phys. Rep. **305**, 203 (1998).

[5] N. L. Manakov, M. V. Frolov, B. Borca, and A. F. Starace, J. Phys. B **36**, R49 (2003).

[6] P. Lambropoulos, G. Doolen, and S. P. Rountree, Phys. Rev. Lett. **34**, 636 (1975).

[7] M. Ya. Agre, V. D. Ovsyannikov, and L. P. Rappoport, Zh. Eksp. Teor. Fiz. **83**, 2027 (1982) [Sov. Phys. JETP **56**, 1174 (1983)].

[8] A. Lyras, B. Dai, X. Tang, P. Lambropoulos, A. Dodhy, J. A. D. Stockdale, D. Zei, and R. N. Compton, Phys. Rev. A **37**, 403 (1988).

[9] F. Lépine, S. Zamith, A. de Snaijer, Ch. Bordas, and M. J. J. Vrakking, Phys. Rev. Lett. **93**, 233003 (2004).

[10] N. Berrah, J. Bozek, J. T. Costello, S. Düsterer, L. Fang, J. Feldhaus, H. Fukuzawa, M. Hoener, Y. H. Jiang, and P. Johnsson *et al.*, J. Mod. Opt. **57**, 1015 (2010).

[11] H. A. Bethe and E. E. Salpeter, *Quantum Mechanics of One and Two Electron Atoms* (Springer-Verlag, Berlin, 1957).

[12] O. Hemmers, R. Guillemin, and D. W. Lindle, Radiat. Phys. Chem. **70**, 123 (2004).

[13] R. Guillemin, O. Hemmers, D. W. Lindle, and S. T. Manson, Radiat. Phys. Chem. **75**, 2258 (2006).

[14] M. B. Trzhaskovskaya, V. I. Nefedov, and V. G. Yarzhemsky, At. Data Nucl. Data Tables **77**, 97 (2001).

[15] A. Bechler and R. H. Pratt, Phys. Rev. A **39**, 1774 (1989).

[16] J. W. Cooper, Phys. Rev. A **47**, 1841 (1993).

[17] B. Krässig, M. Jung, D. S. Gemmell, E. P. Kanter, T. LeBrun, S. H. Southworth, and L. Young, Phys. Rev. Lett. **75**, 4736 (1995).

[18] M. Jung, B. Krässig, D. S. Gemmell, E. P. Kanter, T. LeBrun, S. H. Southworth, and L. Young, Phys. Rev. A **54**, 2127 (1996).

[19] B. Krässig, J.-C. Bilheux, R. W. Dunford, D. S. Gemmell, S. Hasegawa, E. P. Kanter, S. H. Southworth, L. Young, L. A. LaJohn, and R. H. Pratt, Phys. Rev. A **67**, 022707 (2003).

[20] H. R. Varma, M. F. Ciappina, N. Rohringer, and R. Santra, Phys. Rev. A **80**, 053424 (2009).

[21] V. Florescu, O. Budriga, and H. Bachau, Phys. Rev. A **84**, 033425 (2011).

[22] M. Dondera and H. Bachau, Phys. Rev. A **85**, 013423 (2012).

[23] V. Florescu, O. Budriga, and H. Bachau, Phys. Rev. A **86**, 033413 (2012).

[24] E. Koval, S. Fritzsche, and A. Surzhykov, J. Phys. B **37**, 375 (2004).

[25] H. Bachau and P. Lambropoulos, Phys. Rev. A **44**, R9 (1991).

[26] P. Lambropoulos, L. A. A. Nikolopoulos, M. G. Makris, and A. Mihelič, Phys. Rev. A **78**, 055402 (2008).

[27] A. N. Grum-Grzhimailo, E. V. Gryzlova, and M. Meyer, J. Phys. B **45**, 215602 (2012).

[28] E. V. Gryzlova, A. N. Grum-Grzhimailo, S. I. Strakhova, and M. Meyer, J. Phys. B **46**, 164014 (2013).

[29] T. E. Glover, R. W. Schoenlein, A. H. Chin, and C. V. Shank, Phys. Rev. Lett. **76**, 2468 (1996).

[30] P. M. Paul, E. S. Toma, P. Breger, G. Mullot, F. Augé, Ph. Balcou, H. G. Muller, and P. Agostini, Science **292**, 1689 (2001).

[31] S. A. Aseyev, Y. Ni, L. J. Frasinski, H. G. Muller, and M. J. J. Vrakking, Phys. Rev. Lett. **91**, 223902 (2003).

[32] P. O'Keeffe, R. Lopez-Martens, J. Mauritsson, A. Johansson, A. L'Huillier, V. Véniard, R. Taïeb, A. Maquet, and M. Meyer, Phys. Rev. A **69**, 051401 (2004).

[33] O. Guyétand, M. Gisselbrecht, A. Huetz, P. Agostini, R. Taïeb, V. Véniard, A. Maquet, L. Antonucci, O. Boyko, C. Valentin, and D. Douillet, J. Phys. B **38**, L357 (2005).

[34] K. Varjú, P. Johnsson, J. Mauritsson, T. Remetter, T. Ruchon, Y. Ni, F. Lépine, M. Kling, J. Khan, K. J. Schafer, M. J. J. Vrakking, and A. L'Huillier, J. Phys. B **39**, 3983 (2006).

[35] O. Guyétand, M. Gisselbrecht, A. Huetz, P. Agostini, R. Taïeb, A. Maquet, B. Carré, P. Breger, O. Gobert, and D. Garzella *et al.*, J. Phys. B **41**, 051002 (2008).

[36] L. H. Haber, B. Doughty, and S. R. Leone, J. Phys. Chem. A **113**, 13152 (2009).

[37] L. H. Haber, B. Doughty, and S. R. Leone, Phys. Rev. A **84**, 013416 (2011).

[38] B. Doughty, L. H. Haber, C. Hackett, and S. R. Leone, J. Chem. Phys. **134**, 094307 (2011).

[39] M. Meyer, D. Cubaynes, P. O'Keeffe, H. Luna, P. Yeates, E. T. Kennedy, J. T. Costello, P. Orr, R. Taïeb, and A. Maquet *et al.*, Phys. Rev. A **74**, 011401(R) (2006).

[40] M. Meyer, D. Cubaynes, D. Glijer, J. Dardis, P. Hayden, P. Hough, V. Richardson, E. T. Kennedy, J. T. Costello, and P. Radcliffe *et al.*, Phys. Rev. Lett. **101**, 193002 (2008).

[41] M. Meyer, J. T. Costello, S. Düsterer, W. B. Li, and P. Radcliffe, J. Phys. B **43**, 194006 (2010).

[42] V. Richardson, W. B. Li, T. J. Kelly, J. T. Costello, L. A. A. Nikolopoulos, S. Düsterer, D. Cubaynes, and M. Meyer, J. Phys. B **45**, 085601 (2012).

[43] S. Hutchinson, M. A. Lysaght, and H. W. van der Hart, Phys. Rev. A **88**, 023424 (2013).

[44] E. S. Toma and H. G. Muller, J. Phys. B **35**, 3435 (2002).

[45] R. Taïeb, V. Véniard, A. Maquet, N. L. Manakov, and S. I. Marmo, Phys. Rev. A **62**, 013402 (2000).

[46] A. Maquet and R. Taïeb, J. Mod. Opt. **54**, 1847 (2007).

[47] S. Baier, A. N. Grum-Grzhimailo, and N. M. Kabachnik, J. Phys. B **27**, 3363 (1994).

[48] A. N. Grum-Grzhimailo, J. Phys. B **34**, L359 (2001).

[49] S. Devons and L. J. B. Goldfarb, in *Handbuch der Physik*, edited by S. Flügge (Springer-Verlag, Berlin, 1957), Vol. XLII, p. 362.

[50] A. J. Ferguson, *Angular Correlation Methods in Gamma-Ray Spectroscopy* (North-Holland, Amsterdam, 1965).

[51] V. V. Balashov, A. N. Grum-Grzhimailo, and N. M. Kabachnik, *Polarization and Correlation Phenomena in Atomic Collisions* (Kluwer Academic/Plenum Publishers, New York, 2000).

[52] D. D. Varshalovich, A. N. Moskalev, and V. K. Khersonskii, *Quantum Theory of Angular Momentum* (World Scientific, Singapore, 1988).

[53] A. N. Grum-Grzhimailo, J. Phys. B **36**, 2385 (2003).

[54] E. Janke, F. Emde, and F. Lösch, *Tables of Higher Functions* (McGraw-Hill, New York, 1960).

[55] R. L. Chien, O. C. Mullins, and R. S. Berry, Phys. Rev. A **28**, 2078 (1983).

[56] O. C. Mullins, R.-L. Chien, J. E. Hunter, J. S. Keller, and R. S. Berry, Phys. Rev. A **31**, 321 (1985).

[57] P. Radcliffe, S. Düsterer, A. Azima, W. B. Li, E. Plönjes, H. Redlin, J. Feldhaus, P. Nicolosi, L. Poletto, and J. Dardis *et al.*, Nucl. Instrum. Methods A **583**, 516 (2007).

[58] P. Lambropoulos, Phys. Rev. Lett. **28**, 585 (1972).

[59] S. Klarsfeld and A. Maquet, Phys. Rev. Lett. **29**, 79 (1972).

[60] A. Derevianko, W. R. Johnson, and K. T. Cheng, At. Data Nucl. Data Tables **73**, 153 (1999).

[61] T. Mercouris, Y. Komninos, S. Dionissopoulou, and C. A. Nicolaides, Phys. Rev. A **50**, 4109 (1994).

[62] L. A. A. Nikolopoulos, Phys. Rev. A **73**, 043408 (2006).

[63] C. Froese Fischer, T. Brage, and P. Jönsson, *Computational Atomic Structure: An MCHF Approach* (Institute of Physics Publishing, Bristol, 1997).